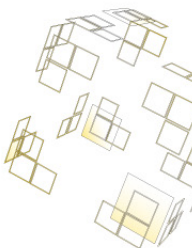


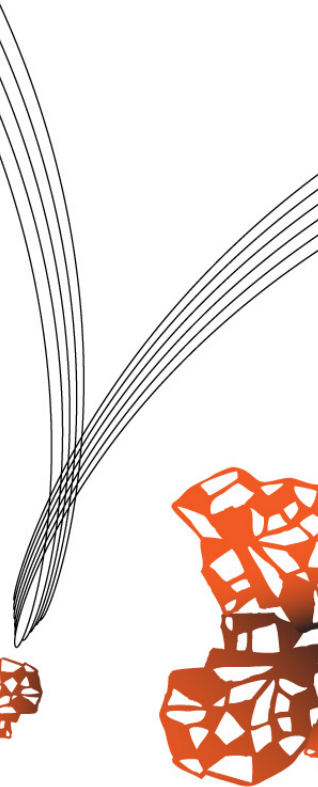


Internship report

A study in beamforming and DAMAS deconvolution



A.J. Bosscha



May 8, 2013

UNIVERSITEIT TWENTE.

Abstract

Aeroacoustic wind tunnel experiments are nowadays performed with phased array measurements. A large array of microphones captures data and together this data can be processed to gain insight the behaviour of the acoustic sources of the test subject. The regular way to process this data is by conventional beamforming. Comparing the cross spectra of the microphones with a reference monopole source tells a lot of the acoustic sources the test object produces.

Using this beamforming data in the DAMAS deconvolution method gives even better insight in acoustic behaviour. DAMAS deconvolution is an iterative method which can predict the locations of acoustic sources in a much better way than conventional beamforming.

There are two possible ways to extract amplitude of sources out of conventional beamforming or DAMAS plots; using an integration method or using the peak levels of the plot. When investigating line sources, the peak level method gives an off result. The height of this off result seems to differ for various coherent lengths of the line source.

A calibration function is made, which compensates for this off result, so the peak level method can also be used to find the strength of line sources. This calibration function is made for several coherent lengths.

Also a method is discussed to extract coherence length out of experimental data. However, this can only be done on a visual manner, therefore the possibility of making an error is high. Due to this error in coherence length estimation, the wrong calibration value can be picked, which results in an error up to 2dB.

Keywords: Beamforming - DAMAS - Coherence - Line source - Peak levels

NOMENCLATURE

$A_{nn'}$	Influence of beamforming characteristics between grid points n and n'
B	Beamwidth
$G_{mm'}$	Cross spectrum between microphone m and m'
I	Sound intensity
M	Mach number
N	Total number of grid points
\cdot'	Fluctuation of variable \cdot
\cdot^H	Hermitian operator
i	Imaginary unit; $\sqrt{-1}$
\hat{A}	DAMAS matrix with $A_{nn'}$ components
ω	Angular frequency
ρ	Density
\hat{G}	Cross Spectral Matrix (CSM)
\hat{d}	Steering vector
\hat{e}	Steering vector
u	Velocity
c	Speed of sound
f	Frequency [Hz]
m	Microphone identity number in the array
m'	Same as m , but independant varied
m_0	Total number of microphones in the array
n	Grid point identity number in the array
n'	Same as n , but independant varied
p	Pressure
t	Time

CONTENTS

1	Introduction	3
2	Sound propagation	5
2.1	Wave equation	5
2.2	Harmonic point source	7
3	Coherence	8
3.1	Interference	8
3.2	Wave trains	8
4	Beamforming	11
4.1	Fundamentals of conventional beamforming	11
4.2	Cross Spectral Matrix data	13
4.3	Accounting for uniform flow	13
4.4	Sidelobes	14
4.5	Noise and reflections	14
5	DAMAS deconvolution	17
5.1	Defenition inverse problem	17
5.2	Solution inverse problem	18
5.3	Application parameters	19
5.4	DAMAS results	19
6	Experimental set-up	23
6.1	Coherent line source	23
6.2	Synthetic CSM	23
6.3	Wind tunnel dimensions	23
6.4	Array	24
6.5	Results	24
7	Array Calibration Function	27
8	Determination of coherence levels	29
8.1	Incoherent monopoles	29
8.2	Line source	29
9	Conclusion	33
9.1	Postscript	33

1. Introduction

The last 100 years a lot has changed in our ways of transportation. In the past men had to use roads, railways or waterways to transport passengers and goods, but since the invention of the aircraft a whole new era begun.

Nowadays aircraft are widely used for transportation. The whole world is easily accesible for work or vacations. This great increase in aircraft usage however, also has some downsides. Commercial airfields, usually located in densed areas, are coping with noise problems. An aircraft at takeoff or landing produces quite an amount of noise, and with lots of departing and arricing flights per airfield, the people (and animals) living nearby are having quite some noise pollution. This is why airfields have to comply with strict noise regulations.

If an aircraft produces less noise at takeoff or landing, the effective capacity of the airfield increases, which means more profit for the airfield and economical growth for the whole region. At the takeoff of an airplane, the turbines are the dominant factor in the production of sound. At the landing however, the sound produced by the wings (flap and slat) and landing gear are the dominating sources.

Aircraft manufacturer Embraer and the aeronautica group of the University of São paulo together have started a collaboration project - the Silent Aircraft Project. The goal of this project is to investigate (and reduce) the sound created by flap, slat and landing gear of Embraer aircrafts. To gain insight in the behaviour of flap, slat, and landing gear induced sound, both numerical simulations and wind tunnel experiments are performed.

Nowadays acoustic wind tunnel experiments are performed with a microphone array. The data from a great amount of microphones is combined to find the acoustic behaviour of the test subject. The difference in phase and amplitude of the different microphone signals is used to find location and amplitude of the sound sources, therefore this technique is called phased array testing.

The data processing thechnique used to locate sound sources and amplitudes is called Conventional Beamforming. This process can acquire, given a certain grid, the locations where there is a high probability of finding an acoustic source. However, this technique has some downsides; the peak levels of line sources are presented wrong for example [1].

To gain even better insight in acoustic behaviour a method called DAMAS deconvolution is used [4]. This method uses the conventional beamfoming spatial plots for its expectation of source locations. The spatial detail of this method is much larger than the results of the conventional beamforming plots. However, also DAMAS deconvolution copes with the problem the peak levels of line sources are wrong.

To solve this problem a calibration function is made. For different frequencies the off-result is calculated, so we get an insight how much the conventional beamforming of DAMAS deconvolution method is off. Not only frequency seems to have an influence in the value of the error, but the coherence length

of the line source also seems to contribute. Therefore the calibration function is made for several coherent lengths of line sources.

Also a method is discussed to extract the coherence length of a line source from wind tunnel experiments. A modified beamforming algorithm is used to compare the coherence of a certain grid point with a reference point.

2. Sound propagation

Sound can be seen as a weak pressure disturbance which travels through a fluid. The perturbation moves through the fluid as a wave and causes small variations in the velocity and density of the fluid.

Although the acoustic pressure fluctuations are small compared to the mean (atmospheric) pressure, the range in amplitudes is very large. This makes it convenient to express pressure amplitude p on the logarithmic scale:

$$SPL(dB) = 20 \log \frac{p_{rms}}{p_{ref}} \quad (2.1)$$

where SPL is the sound pressure level in decibels, p_{rms} the root-mean-squared value of the pressure and p_{ref} the reference pressure of $2 \cdot 10^5 Pa$.

Since disturbances are small, the variables have to satisfy the linearized equations of fluid motion. For sound propagation inertial forces are usually much larger than viscous forces. Effects of viscosity can therefore be neglected when examining acoustic wave propagation.

2.1 Wave equation

Consider a fluid with velocity \mathbf{u}_t , density ρ_t and pressure p_t . From the conservation of mass it follows that

$$\frac{\partial \rho_t}{\partial t} + \nabla \cdot (\rho_t \mathbf{u}_t) = 0 \quad (2.2)$$

Conservation of momentum gives

$$\frac{\partial(\rho_t \mathbf{u}_t)}{\partial t} + \nabla \cdot (\rho_t \mathbf{u}_t \mathbf{u}_t) + \nabla P_t = \mathbf{f} \quad (2.3)$$

where ∇ is the nabla operator ($\partial/\partial x, \partial/\partial y, \partial/\partial z$), \mathbf{f} the density of the external force field acting on the fluid and $P_t = p_t \mathbf{I} - \boldsymbol{\tau}$ is the fluid stress tensor. By neglecting viscosity and using the conservation of mass (2.2) the conservation of momentum (2.3) can be written as the Euler equations [5].

$$\rho_t \left(\frac{\partial \mathbf{u}_t}{\partial t} + \mathbf{u}_t \cdot \nabla \mathbf{u}_t \right) + \nabla p_t = \mathbf{f} \quad (2.4)$$

Considering small perturbations of velocity, pressure and density, equation (2.2) and equation (2.4) can be linearized. We write $\mathbf{u}_t = \mathbf{u}_0 + \mathbf{u}$, $p_t = p_0 + p$ and $\rho_t = \rho_0 + \rho$, where the subscript '0' indicates the uniform mean value and the quantity without subscript represent the fluctuations. Assuming a constant

mean velocity $\mathbf{u}_0 = \mathbf{U}$ and $\mathbf{f} = 0$, the linearized equations for conservation of mass and momentum can be rewritten as

$$\frac{\partial \rho}{\partial t} + \mathbf{U} \cdot \nabla \rho + \rho_0 \nabla \cdot \mathbf{u} = 0 \quad (2.5a)$$

$$\rho_0 \left(\frac{\partial \mathbf{u}}{\partial t} + \mathbf{U} \cdot \nabla \mathbf{u} \right) + \nabla p = 0 \quad (2.5b)$$

If the uniform quantities \mathbf{U} , p_0 and ρ_0 are known, equations (2.5) only provide four equations for the five unknowns \mathbf{u} , p and ρ . The additional information can be found in the constitutional equations. We assume the fluid to be in a state of thermodynamic equilibrium. This means we can write the pressure p_t as a function of the density ρ_t and entropy s_t .

$$dp_t = \left(\frac{\partial p_t}{\partial \rho_t} \right)_s d\rho_t + \left(\frac{\partial p_t}{\partial s_t} \right)_\rho ds_t \quad (2.6)$$

Momentum and heat transfer are controlled by the same molecular collisional process. If we neglect viscosity, we should also neglect heat transfer, and therefore the flow is isentropic. This means the entropy of a fluid particle remains constant and therefore $ds_t = 0$. By defining the speed of sound as $c^2 = (\partial p_t / \partial \rho_t)_s$, equation (2.6) becomes

$$p = c_0^2 \rho \quad (2.7)$$

where $c_0 = c(p_0, \rho_0)$ is used to approximate the speed of sound c .

Using equation (2.7) we can write ρ in terms of p . Using this in equation (2.5a) and subtracting the divergence of equation (2.5b), velocity \mathbf{u} is eliminated and the convective wave equation is obtained.

$$\frac{1}{c_0^2} \left(\frac{\partial}{\partial t} + \mathbf{U} \cdot \nabla \right)^2 p - \nabla^2 p = 0 \quad (2.8)$$

For many applications this equation can be simplified by assuming zero mean flow ($\mathbf{U} = 0$). This equation is called the wave equation of d'Alembert.

$$\frac{1}{c_0^2} \frac{\partial^2 p}{\partial t^2} - \nabla^2 p = 0 \quad (2.9)$$

Transforming d'Alembert's wave equation to spherical coordinates and assuming the pressure field is axi-symmetric gives the following equation. The product rp satisfies the one-dimensional wave equation.

$$\frac{1}{c_0^2} \frac{\partial^2 rp}{\partial t^2} - \frac{\partial^2 rp}{\partial r^2} = 0 \quad (2.10)$$

Solving this equation gives the expression for an outward propagating harmonic spherical wave.

$$p(r, t) = \frac{Ae^{i\omega(t-r/c_0)}}{r} \quad (2.11)$$

This wave travels outward at speed c_0 . Its amplitude is inversely proportional to the distance.

2.2 Harmonic point source

Up now we have considered propagating waves whose behaviour is governed by the homogeneous wave equation (2.9). This equation however, only describes the propagation of sound generated at boundaries, incoming sound fields from infinity or sound due initial perturbations. A sound source $q(\mathbf{x}, t)$ is defined, which produces sound at a certain location \mathbf{x} .

$$\frac{1}{c_0^2} \frac{\partial^2 p}{\partial t^2} - \nabla^2 p = q \quad (2.12)$$

The source region, where q is non-zero, is separated from the sound field, where q is zero and the propagation of sound waves is governed by the homogeneous wave equation. Where q is non-zero the sound field is uniquely determined by the given initial and boundary conditions.

$$q(\mathbf{x}, t) = \delta(\mathbf{x} - \mathbf{x}_s) \sigma_s(t) \quad (2.13)$$

Where δ is the Dirac delta function, which is zero everywhere, and nears infinity when its argument is zero. $\sigma_s(t)$ is the source behaviour.

3. Coherence

In this chapter the meaning of coherence is explained, but to do so first the subject interference will be examined.

3.1 Interference

A pressure field often contains sound waves from different sources. Assume the spatial parts of two pressure waves are described by:

$$p_1 = A_1 e^{-i\phi_1} \quad (3.1a)$$

$$p_2 = A_2 e^{-i\phi_2} \quad (3.1b)$$

where ϕ_1 and ϕ_2 are functions of position and represent the phase shift of the waves. The superposition principle may be applied and the resulting pressure field becomes merely the sum of the two individual fields.

$$p = p_1 + p_2 \quad (3.2)$$

The observed quantity is, however, the sound intensity.

$$\begin{aligned} I &= |p|^2 \\ &= |p_1 + p_2|^2 \\ &= A_1^2 + A_2^2 + 2A_1A_2 \cos(\phi_1 - \phi_2) \\ &= I_1 + I_2 + 2\sqrt{I_1I_2} \cos(\Delta\phi) \end{aligned} \quad (3.3)$$

where $\Delta\phi$ is the difference in phase between the two waves. As it can be seen, the sound intensity does not become merely the sum of the two intensities. The term $2\sqrt{I_1I_2} \cos(\Delta\phi)$ is called the interference term [2].

Detection of sound by a microphone is an averaging process in time. In developing equation (3.3) no averaging over time is done, because it is assumed the phase difference $\Delta\phi$ is constant in time. This also means it is assumed p_1 and p_2 have the same frequency.

3.2 Wave trains

One way to illustrate sound waves emitted by a real source is to picture it as multiple sinusoidal wave trains with finite length, and a randomly distributed phase difference between them. Figure 3.1 shows two wave trains of the partial sound waves described in equations (3.1a) and (3.1b). The two wave trains have equal amplitude and length L_c . Between the two wave trains and

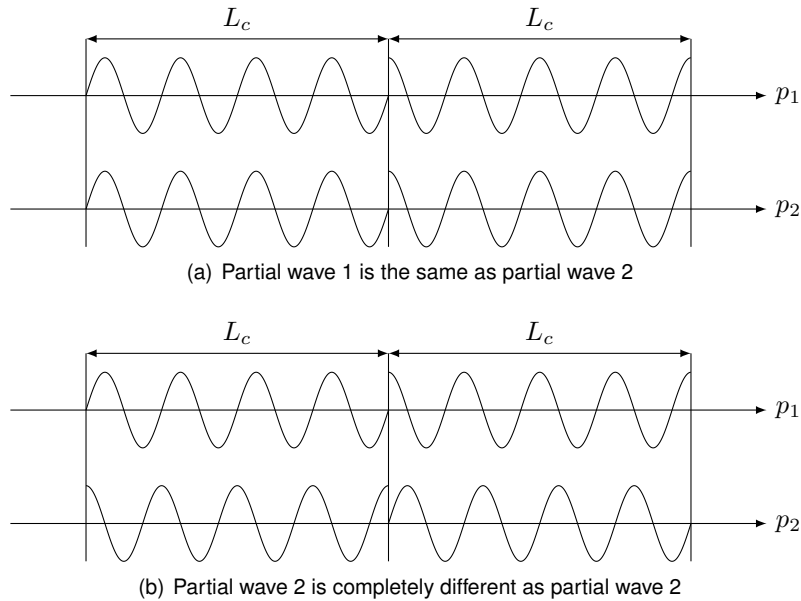


Figure 3.1: Wavetrains

abrupt, arbitrary phase change takes place. In figure 3.1(a) both wave trains have traveled equal distance. Between the two waves, the phase difference is equal in time. The intensity of these waves is given by equation (3.3).

Since the phase difference between the two partial waves is absent, the sound intensity of the field becomes $I_1 + I_2 + 2\sqrt{I_1 I_2}$. When both partial waves have the same sound intensity I_0 , the sound intensity becomes $4I_0$. In this case the partial waves are called fully coherent.

In figure 3.1(b), the second partial wave has traveled exactly one wave train length (L_c) further than the first partial wave. The sound intensity is still given by equation 3.3. The phase difference now fluctuates randomly as the wave trains pass by. This means the part $\cos \Delta\phi$ seen in the interference term fluctuates between -1 and $+1$. When averaged over many wave trains, the interference term becomes zero, and the observed intensity will be $I_1 + I_2$. If both partial waves have the same intensity I_0 , the amplitude of the field becomes $2I_0$. This case is called the incoherent case. Cases between fully coherent and incoherent are called partial coherent. However, in this report only the incoherent and fully coherent cases will be examined.

Figure 3.2 represents a line source. When looking at some points located at the line source at position x_i , we can tell something about the coherence level between these points. When the distance between the two points is small, the level of coherence is usually higher as the coherence level between points which have more distance between them. If the points are close together, they usually emit pressure waves which are much more alike, and thus are more coherent.

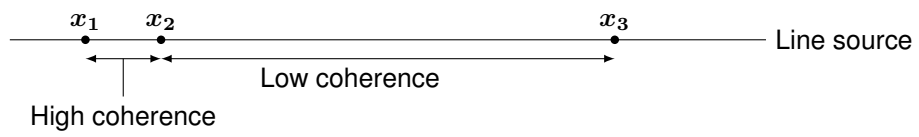


Figure 3.2: Line source

4. Beamforming

In aeroacoustic testing, a model is exposed to a flow. This flow causes the model to produce a complex array of sounds. Often several parts of the model have interesting noise production worth examining. These different sources create sounds in a wide frequency spectrum and different tone.

A technique often used to get an insight in the location and strength of these different sources is phased array testing. In phased array testing, several microphones can be used together to extract source location and strength information from noisy, non-acoustic wind tunnels.

The basic phased array processing step is called beamforming. Beamforming has a long history in radio astronomy, but can also be applied to acoustic problems. The beamforming process uses a mathematical model for the acoustic propagation from each grid point to each microphone. Cross spectral data between different microphones is used to gain insight in acoustic source distribution.

4.1 Fundamentals of conventional beamforming

The general idea of beamforming signal processing is to compare the data measured by the array of microphones with a reference pressure. As reference pressure a harmonic monopole source is taken. By minimizing the squared norm of the difference between these two quantities, a good estimate of the source location and strength is given.

In equation 4.1 \hat{p} represents the spatial pressure component of the reference pressure, a signal emitted by a monopole source at location \mathbf{r}_s at a specific frequency f . The variable a_s represents the complex amplitude of this monopole source, which may vary for different frequencies and positions.

$$\hat{p}(a_s, \mathbf{r}_s, \mathbf{r}) = \frac{a_s e^{-ik|\mathbf{r}-\mathbf{r}_s|}}{4\pi|\mathbf{r}-\mathbf{r}_s|} \quad (4.1)$$

Equation 4.1 can also be written as $\hat{\mathbf{e}}\mathbf{a}_s$, where each term of column vector $\hat{\mathbf{e}}$ represents the reference signal for a different microphone. $\hat{\mathbf{e}}$ is also called the steering vector.

All the k -th Fourier transform coefficients of a real signal recorded by the microphone array are stored in column vector \mathbf{P} . The length of the vector equals the number of microphones. By defining a cost function J (4.2), an estimate of \mathbf{a}_s can be made by minimizing this function.

$$J(\omega, \mathbf{a}_s, \mathbf{r}_s) = \|\hat{\mathbf{e}}\mathbf{a}_s - \mathbf{P}\|^2 \quad (4.2)$$

Using $\mathbf{u} = \hat{\mathbf{e}}\mathbf{a}_s - \mathbf{P}$ and the identity shown below (4.3), the derivative of the cost function (4.2) can be expressed.

$$\frac{d}{d\mathbf{u}}(\mathbf{u}^H \mathbf{u}) = 2\mathbf{u}^H \mathbf{I} \quad (4.3)$$

In this equation I represents the identity matrix.

$$\frac{dJ}{d\mathbf{a}_s} = \frac{dJ}{d\mathbf{u}} \frac{d\mathbf{u}}{d\mathbf{a}_s} = 2(\hat{\mathbf{e}}\mathbf{a}_s - \mathbf{P})^H \hat{\mathbf{e}} \quad (4.4)$$

The cost function is minimal if derivative of it (4.4) is zero. Using the identity $\mathbf{A}^H \mathbf{B} = \mathbf{A} \mathbf{B}^H$ this can be rewritten to:

$$\hat{\mathbf{e}}^H \hat{\mathbf{e}} \mathbf{a}_s = \hat{\mathbf{e}}^H \mathbf{P} \quad (4.5)$$

Which leads to the least square solution of \mathbf{a}_s .

$$\tilde{\mathbf{a}}_s = (\hat{\mathbf{e}}^H \hat{\mathbf{e}})^{-1} \hat{\mathbf{e}}^H \mathbf{P} = \frac{\hat{\mathbf{e}}^H \mathbf{P}}{\|\hat{\mathbf{e}}\|^2} \quad (4.6)$$

Below the cost function J is expanded in terms of \mathbf{a}_s .

$$\begin{aligned} \|\hat{\mathbf{e}}\mathbf{a}_s - \mathbf{P}\|^2 &= (\hat{\mathbf{e}}\mathbf{a}_s - \mathbf{P})(\hat{\mathbf{e}}\mathbf{a}_s - \mathbf{P})^H \\ &= (\mathbf{a}_s^H \hat{\mathbf{e}}^H - \mathbf{P}^H)(\hat{\mathbf{e}}\mathbf{a}_s - \mathbf{P}) \\ &= \mathbf{a}_s^H \hat{\mathbf{e}}^H \hat{\mathbf{e}} \mathbf{a}_s - 2\mathbf{a}_s^H \hat{\mathbf{e}}^H \mathbf{P} + \mathbf{P}^H \mathbf{P} \end{aligned} \quad (4.7)$$

Using the least square solution of \mathbf{a}_s gives:

$$J(\omega, \mathbf{r}_s) = \mathbf{P}^H \mathbf{P} - \frac{(\hat{\mathbf{e}}^H \mathbf{P})^H (\hat{\mathbf{e}}^H \mathbf{P})}{\hat{\mathbf{e}}^H \hat{\mathbf{e}}} \quad (4.8)$$

The term $\mathbf{P}^H \mathbf{P}$ represents the sum of all auto spectra of the array. Because it is derived directly from the external sound field, it does not depend on the parameters used to model the acoustic field, and can be seen as a constant in this formulation.

$$\begin{aligned} I(\omega, \mathbf{r}_s) &= \frac{(\hat{\mathbf{e}}^H \mathbf{P})^H (\hat{\mathbf{e}}^H \mathbf{P})}{\hat{\mathbf{e}}^H \hat{\mathbf{e}}} \\ &= \frac{\hat{\mathbf{e}}^H}{\|\hat{\mathbf{e}}\|} \mathbf{P} \mathbf{P}^H \frac{\hat{\mathbf{e}}}{\|\hat{\mathbf{e}}\|} \\ &= \frac{\hat{\mathbf{e}}^H}{\|\hat{\mathbf{e}}\|} \hat{\mathbf{G}} \frac{\hat{\mathbf{e}}}{\|\hat{\mathbf{e}}\|} \end{aligned} \quad (4.9)$$

The matrix $\hat{\mathbf{G}}$ is called the cross spectral matrix (CSM), and contains the time averaged data of the microphones. When there are m_0 microphones used in the array, $\hat{\mathbf{G}}$ will have an $m_0 \times m_0$ size.

$$\hat{\mathbf{G}} = \begin{bmatrix} G_{11} & G_{12} & \cdots & G_{1m_0} \\ \vdots & G_{22} & & \vdots \\ \vdots & & \ddots & \vdots \\ G_{m_0 1} & \cdots & \cdots & G_{m_0 m_0} \end{bmatrix} \quad (4.10)$$

By maximizing imaging function I , the cost function J is minimized. In practice, the function I is estimated over a discrete mesh domain to create one spatial map of beamforming for each scanning frequency. In the final beamforming map, the strongest peaks indicate the regions in which there is a high probability of finding sound sources.

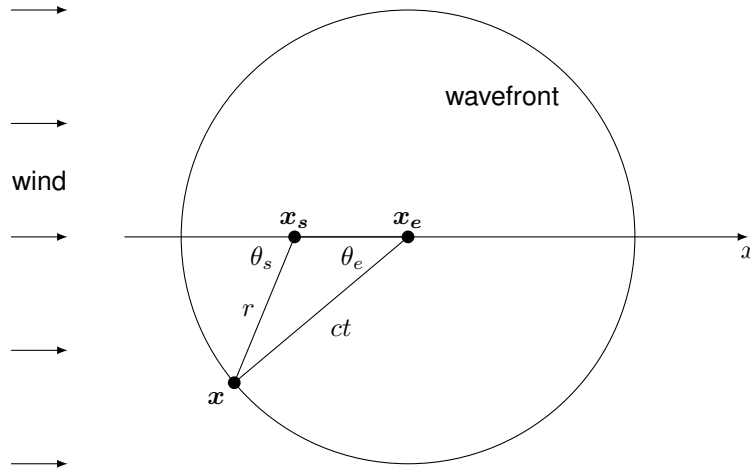


Figure 4.1: Wavefront in uniform flow

4.2 Cross Spectral Matrix data

When doing wind tunnel experiments, large amounts of data are obtained. All microphones gather data during the time of the experiment T_{tot} . To gain insight in the acoustic behaviour of the flow, the data is time averaged. As stated in section 4.1, first the Fourier transform of each microphone is taken. This gives different data sets per frequency f , which are Δf apart from each other. Afterwards, each data sample is divided into several blocks of time T .

$$G_{mm'}(f) = \frac{2}{K w_s T} \sum_{k=1}^K [P_{mk}^T(f, T) P_{m'k}(f, T)] \quad (4.11)$$

The cross spectrum is averaged over K block averages. The term w_s is a data window weighting constant - often Hamming windowing is used.

4.3 Accounting for uniform flow

In the determination of steering vector \hat{e} , it is assumed the sound waves pass through a non-moving medium. However, in windtunnel experiments the medium (air) moves at a certain speed U . To take account for this, a correction to steering vector is made.

Assume the time it takes for a sound wave to travel from the source to the microphone, in the non-moving medium case is Δt . When the medium moves uniformly at a certain speed U , the sound waves travel a distance $U \Delta t$ downstream.

Figure 4.1 gives a schematic overview of the situation. x_s is the location of the source. Because the sound waves move downstream, the observer x thinks the source is located at x_e .

Rewriting this in terms of mach number M , gives a new corrected steering vector.

$$\hat{e} = \frac{R}{r_c} e^{-i2\pi f T} \quad (4.12)$$

Where R and r_c are corrected with the Doppler amplification factor $1 - M^2$. r_c is the corrected distance from the observing point to the center of the coordinate system.

$$r_c = \sqrt{x^2 + (1 - M^2)(y^2 + z^2)} \quad (4.13)$$

R is the corrected distance from observing point the the source location.

$$R = \sqrt{(x - x_s)^2 + (1 - M^2)((y - y_s)^2 + (z - z_s)^2)} \quad (4.14)$$

$$T = \frac{-M(x - x_s) + R}{(1 - M^2)c} \quad (4.15)$$

Using this steering vector \hat{e} the system is adapted for uniform flow of mach number M .

4.4 Sidelobes

The output of the beamform algorithm relies ofcourse on the sound sources. However, when sound source is taken constant, differences in the spatial beamforming map can be seen for different frequencies and array designs. At higher frequencies, small peaks can be seen on locations that are not at a sound source. These small peaks are called sidelobes. The main lobe is the is the peak resulting from the sound source.

In figure 4.2 the sidelobe effect can be seen for different frequencies. The figures clearly show the sidelobe effect increases for increasing frequencies. At 5000Hz almost no sidelobes are seen, but at 20000Hz the sidelobes are almost at the same strength as the main lobe.

The sidelobe effect can be resolved my putting a treshold on the beamforming map. Every value which is a set value lower that the highest peak level, gets removed. This treshold is often called dynamic range. It should be noticed that by using a treshold, it is also possible to remove main lobes with less strenght than the strongest main lobe.

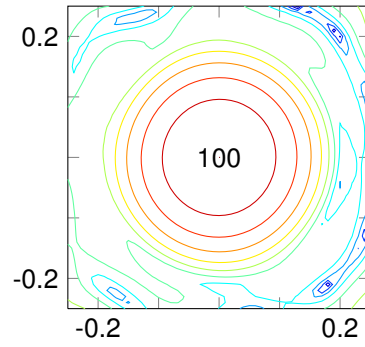
4.5 Noise and reflections

When performing acoustic experiments, it is impossible to have the perfect conditions. All kind of imperfections make it difficult to compare experimental results with the theory, which asumes a perfect anechoic wind tunnel facility and no noise.

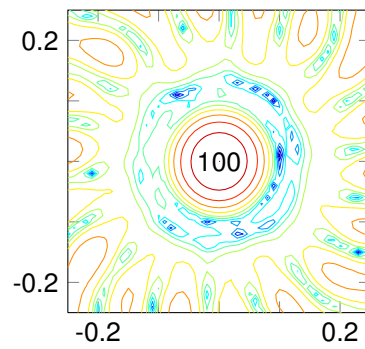
No windtunnel is completely anechoic, so the microphone array will notice the reflections of the sound waves against the wind tunnel walls. However, using good isolation against the walls these reflections can be greatly reduced. Reflections of sources are fully coherent with their original source. In chapter 8 this property is used to to find reflections or sidelobes.

Intermittend sounds, like people talking outside the windtunnel, are random and can be took out by time averaging.

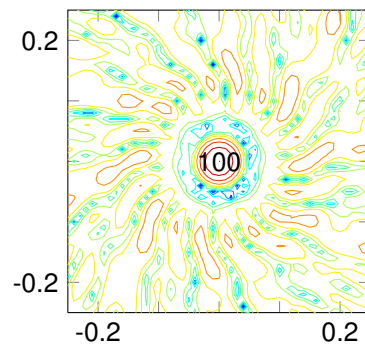
The microphones are usually flush-mounted in the wall. At the wall, a turbulent boundary layer occurs. The microphones will therefore detect the hydrodynamic pressure fluictuations caused by the boundary layer. Since this



(a) 5000Hz



(b) 10000Hz



(c) 20000Hz

Figure 4.2: Sidelobes at different frequencies

noise is generally incoherent from one microphone to the other, it will only appear in the auto spectra of the CSM. Removing the auto powers (Diagonal Removal) of the CSM, can remove this floor of noise from the beamforming spatial maps.

The suspension of the test subject often causes fluctuation in the flow, and therefore pressure fluctuations. This is a problem that cannot be overcome.

5. DAMAS deconvolution

The processing of array data with the conventional beamforming technique (chapter 4) is burdened with considerable uncertainty. The Deconvolution Approach for the Mapping of Acoustic Sources (DAMAS) removes beamform characteristics from the output presentation. Using the DAMAS deconvolution method, misinterpretations are reduced when quantifying position and strength of acoustic sources.

First an inversed beamforming problem is defined, which results in a set of linear independent equations. Afterwards these equations are solved using a special iterative algorithm.

5.1 Defenition inverse problem

The pressure transform P_m of microphone m is related to a modeled monopole source located at position n .

$$P_{m:n} = Q_n e_{m:n}^{-1} \quad (5.1)$$

The term $e_{m:n}^{-1}$ is simply the inversed steering vector. The product of pressure transforms now becomes

$$\begin{aligned} P_{m:n}^T P_{m':n} &= (Q_n e_{m:n}^{-1})^T (Q_n e_{m':n}^{-1}) \\ &= Q_n^T Q_n (e_{m:n}^{-1})^T e_{m':n}^{-1} \end{aligned} \quad (5.2)$$

When all there cross spectra are stored in a matrix, the modified CSM $\hat{G}_{n_{mod}}$ for a modeled source at grid point n is obtained. This CSM only contains data from grid point n .

$$\hat{G}_{n_{mod}} = X_n \begin{bmatrix} (e_1^{-1})^T e_1^{-1} & (e_1^{-1})^T e_2^{-1} & \dots & (e_1^{-1})^T e_{m_0}^{-1} \\ (e_2^{-1})^T e_1^{-1} & (e_2^{-1})^T e_2^{-1} & & \vdots \\ & & \ddots & \vdots \\ & & & (e_{m_0}^{-1})^T e_{m_0}^{-1} \end{bmatrix} \quad (5.3)$$

Taking the sum over all grid points, gives the total modified CSM \hat{G}_{mod} .

$$\hat{G}_{mod} = \sum_n \hat{G}_{n_{mod}} \quad (5.4)$$

Using this modified CSM in the conventional beamforming expression (equation 4.9) gives:

$$\begin{aligned}
I_{n_{mod}}(\hat{e}) &= \left[\frac{\hat{e}^H}{\|\hat{e}\|} \hat{G}_{mod} \frac{\hat{e}}{\|\hat{e}\|} \right]_n \\
&= \frac{\hat{e}_n^H}{\|\hat{e}_n\|} \sum_{n'} \hat{X}_{n'} [\dots]_{n'} \frac{\hat{e}_n}{\|\hat{e}_n\|} \\
&= \sum_{n'} \frac{\hat{e}_n^H}{\|\hat{e}_n\|} [\dots]_{n'} \frac{\hat{e}_n}{\|\hat{e}_n\|} \hat{X}_{n'}
\end{aligned} \tag{5.5}$$

Where the bracketed term is the matrix stated in equation 5.3. This expression can be rewritten to:

$$I_{n_{mod}}(\hat{e}) = \sum_{n'} A_{nn'} \hat{X}_{n'} \tag{5.6}$$

With

$$A_{nn'} = \frac{\hat{e}_n^H}{\|\hat{e}_n\|} [\dots]_{n'} \frac{\hat{e}_n}{\|\hat{e}_n\|} \tag{5.7}$$

By equating $I_{n_{mod}}(\hat{e})$ with processed from measured data $I(\hat{e}) = I_n$, we have

$$\hat{A} \hat{X} = \hat{I} \tag{5.8}$$

The matrices \hat{A} , \hat{X} and \hat{I} have components $A_{nn'}, X_n$ and Y_n , respectively.

5.2 Solution inverse problem

Equation 5.8 is a system of linear equations. If matrix \hat{A} would be non-singular, the solution would be $\hat{X} \hat{A}^{-1} = \hat{I}$. For the present acoustic problems of interest however, the matrix \hat{A} is usually ill conditioned (singular).

Special iterative solving methods, such as Conjugate Gradient method and other did not give satisfactory results.

With the assumption the sources X_n are statistically independent, leading to equation 5.8, it is known that X_n should all have a positive value. Using this constraint in a very simple iterative method gave very good results [4]. This iterative method is described below.

A single equation component of equation 5.8 is given by:

$$A_{n1}X_1 + A_{n2}X_2 + \dots + A_{nn}X_n + \dots + A_{nN}X_N = I_n \tag{5.9}$$

Rearranging and using $A_{nn} = 1$ gives:

$$X_n = Y_n - \left[\sum_{n'=1}^{n-1} A_{nn'} X_{n'} + \sum_{n'=n+1}^N A_{nn'} X_{n'} \right] \tag{5.10}$$

This equation is used in an iteration algorithm to find the source distribution X_n for all grid points. The iteration algorithm is described below, where (i) is the iteration index.

$$\begin{aligned}
X_1^{(i)} &= Y_1 - \left[0 + \sum_{n'=1}^N A_{1n'} X_{n'}^{(i-1)} \right] \\
X_n^{(i)} &= Y_n - \left[\sum_{n'=1}^{n-1} A_{nn'} X_{n'}^{(i)} + \sum_{n'=n+1}^N A_{nn'} X_{n'}^{(i-1)} \right] \\
X_N^{(i)} &= Y_N - \left[\sum_{n'=1}^{N-1} A_{Nn'} X_{n'}^{(i)} + 0 \right]
\end{aligned} \tag{5.11}$$

For the first iteration ($i = 1$), the initial values are taken $X_n = 0$. However, taking initial value $X_n = I_n$ gives little change in convergence rate. After each $X - n$ determination it is checked if the value is positive (or zero), if it isn't the value is set to zero. This iterative method seems robust and converge to the solution.

It should be noticed the chosen grid space should match beamform characteristics, to give a good distinction between I_n to make the separate equations linear independant. If the values of I_n are close together the system becomes linear dependant and the solutions become off.

5.3 Application parameters

To get fast convergence rates with the DAMAS iterative proces, there should be a good distinction between the beamforming values I_n . To describe this distinction in mathematical terms, the term 'beamwidth' is introduced. The beamwidth B is defined as the diameter of the 3dB down output of the beamform map, compared to its maximum. For convential beamforming

$$B \approx C \left(\frac{R}{fD} \right) \tag{5.12}$$

where R is the distance from the array to the scanning plane, D is the array diameter (figure 5.1) and C a constant.

The parameter ration $\Delta x/B$ and W/B appear to be most important for establishing resolution and spatial extent requirements of the scanning plane.

The resolution $\Delta x/B$ must be fine enough such that individual grid points along with other grid points represent a reasonable physical distribution of sources. However, too fine distribution would require lots of computational effort.

On the other hand, a too coarse distribution would render solutions of \hat{X} which would not show the required spatial detail.

Figure 5.1[4] shows some of the above mentioned parameters.

5.4 DAMAS results

In this section some results from the DAMAS deconvolution method are shown and compared with results from conventional beamforming plots. For different frequencies and number of iterations the results will be plotted.

Figure 5.2 shows the result of a modeled 100dB monopole source located at the center of the grid after 10, 100, and 1000 iterations. Figure 5.3 shows

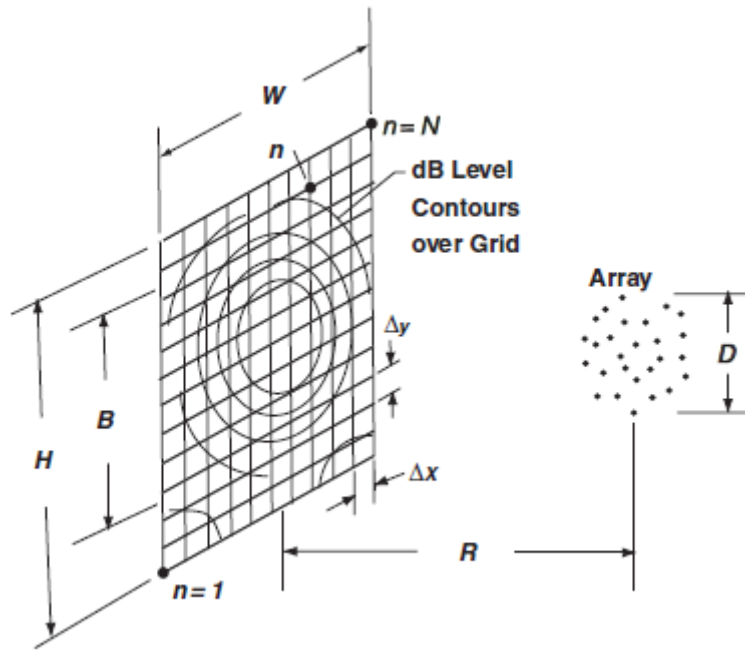


Figure 5.1: DAMAS geometric parameters

Iterations	5000Hz	10000Hz	20000Hz
B	0.1523	0.0800	0.0400
10	80.5982	88.8046	96.0881
100	88.4683	94.9115	99.9566
1000	93.2602	99.7010	99.9977

Table 5.1: Source strength after different iteration numbers

the same experiment at 10000Hz. The results of the experiment at 20000Hz are shown by figure 5.4.

Table 5.1 shows the value of the peak levels of conventional beamforming plots and DAMAS deconvolution. Beamwidth B is also shown.

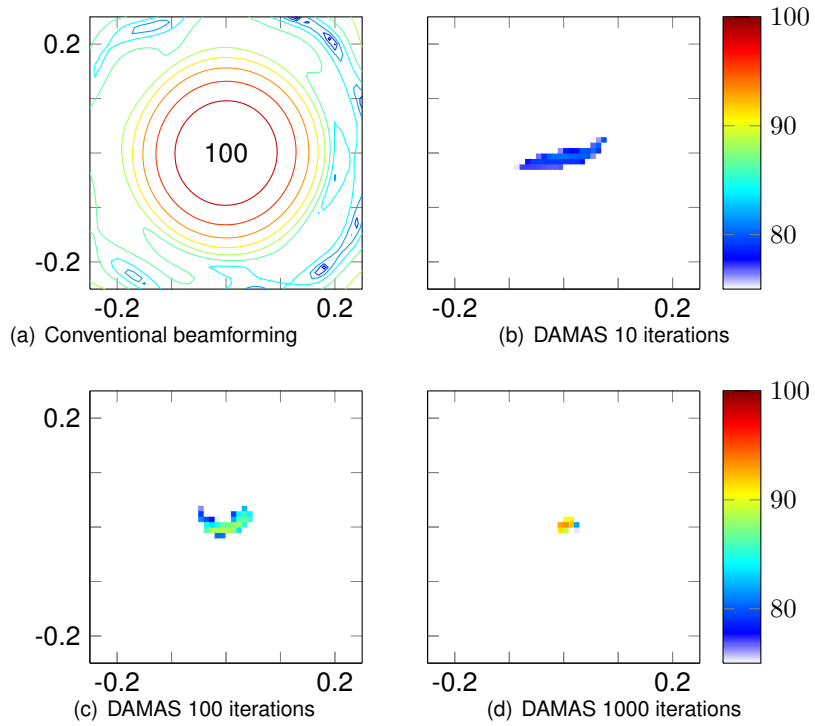


Figure 5.2: DAMAS 5000Hz

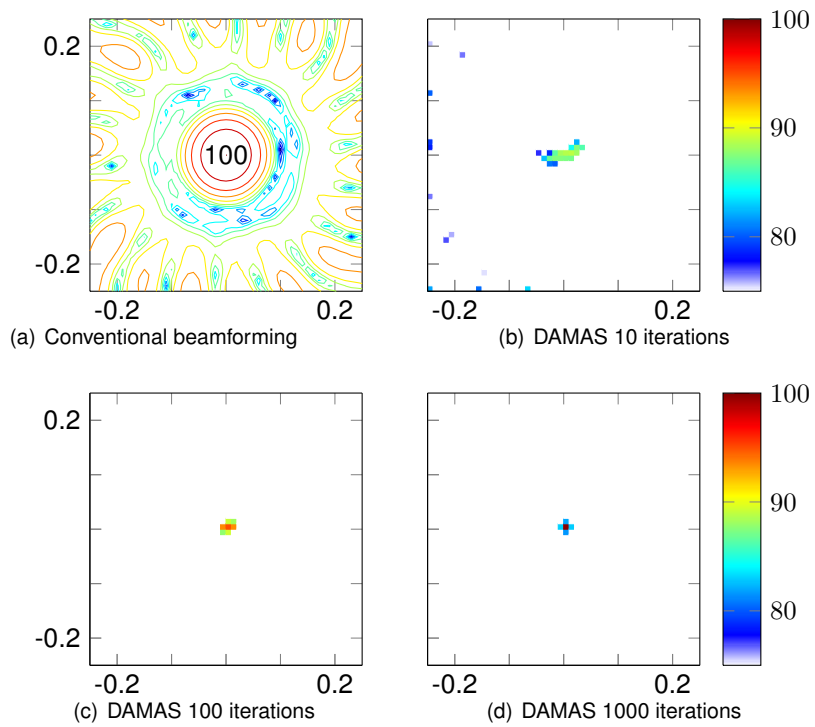


Figure 5.3: DAMAS 10000Hz

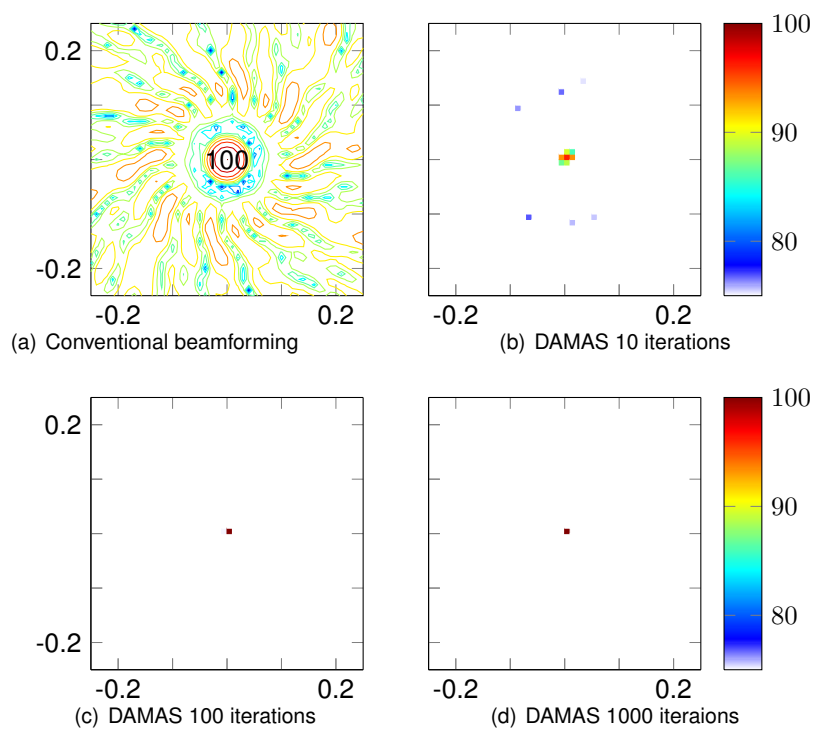


Figure 5.4: DAMAS 20000Hz

6. Experimental set-up

To investigate the behaviour of the beamforming algorithm when processing a line source, an experimental set-up has to be made. The line source is simulated using a line of equidistant monopoles. From these monopoles a synthetic CSM is constructed.

6.1 Coherent line source

The line source is simulated using a set number of equidistant monopoles (harmonic point sources). These monopoles are added to a coherent group (see figure 6.1). All the monopoles in a coherent group are fully coherent with each other, but fully incoherent with the monopoles from other coherent groups. By varying the number of monopoles in a coherent group, different coherent lengths of the line source can be simulated.

The number of sources per length unit is the limiting factor of the lowest coherent length possible to be simulated. The length of the line source gives the limit of the highest coherent length possible to simulate.

6.2 Synthetic CSM

The pressure field the microphones receive can be calculated from the superposition of all pressure fields of the point sources, and taking the coherent terms into account. At the construction of the CSM, only the spatial part of the sources is considered. Only considering the spatial part is equal to taking an infinite number of time averages.

6.3 Wind tunnel dimensions

To match the computational experiments with the wind tunnel in the area acoustic department of the University of São Paulo, the dimensions of the wind tunnel are used for the experiments.

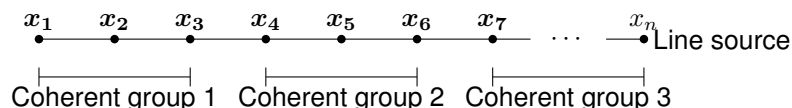


Figure 6.1: Line source model

Number of microphones	63
Distance array-object	0.85m
Height tunnel	1.50m

Table 6.1: Wind tunnel dimensions

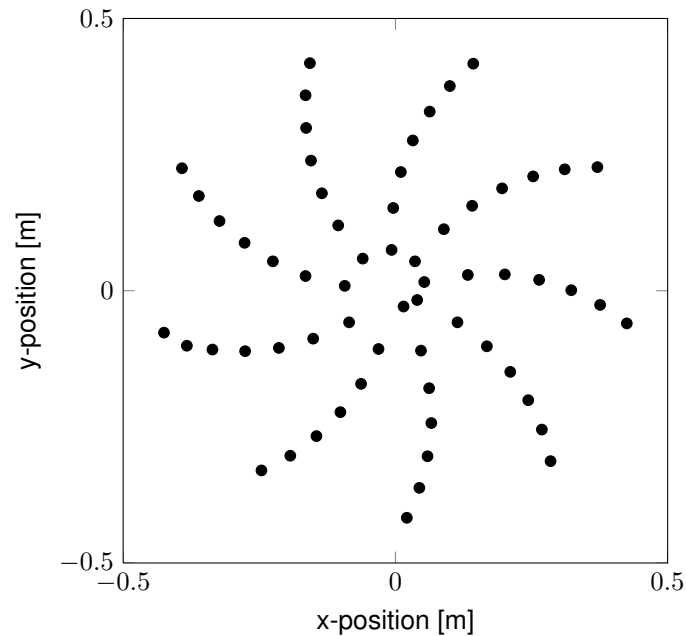


Figure 6.2: 63 microphone array

6.4 Array

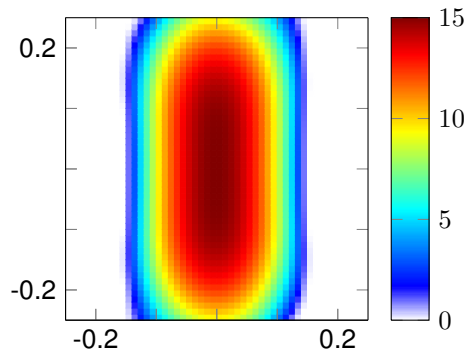
The array setup used is a logarithmic spiral. This setup is proven to work at low as well as high frequency signals [5]. An overview of the array is shown in figure 6.4.

6.5 Results

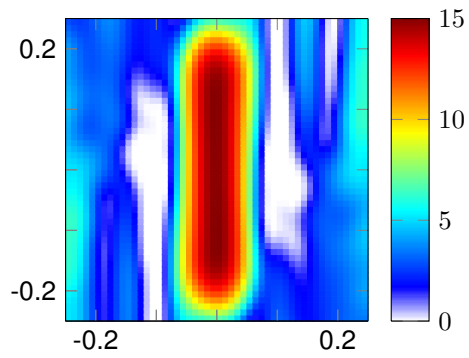
Figure 6.3 shows the beamform plots of an incoherent line source. Shown is the dynamic range, from the top until 15dB down. The plots of the other coherence lengths look the same, only the peak level (which isn't shown in this plot) differs.

The DAMAS plots of the incoherent line source simulation are shown in figure 6.4. It can be seen the sidelobes are clearly more visible in the higher frequency simulations.

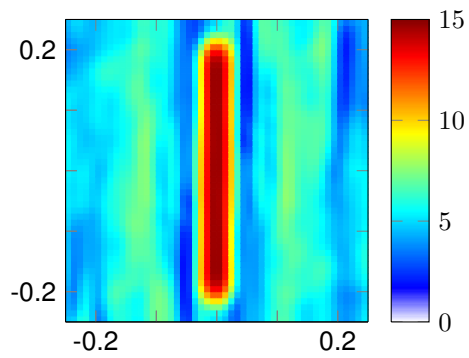
In chapter 7 the peak levels of conventional beamforming and DAMAS plots are examined.



(a) 5000Hz

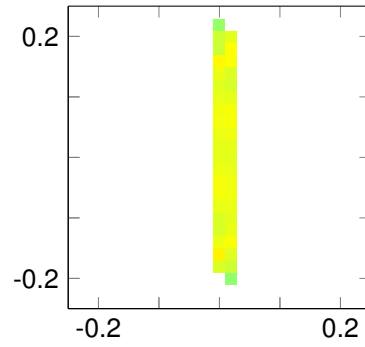


(b) 10000Hz

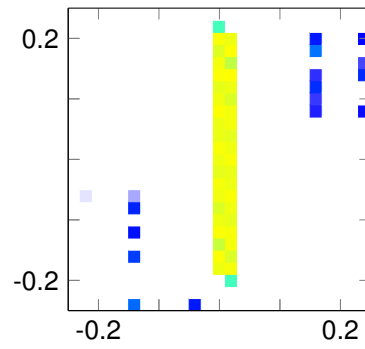


(c) 20000Hz

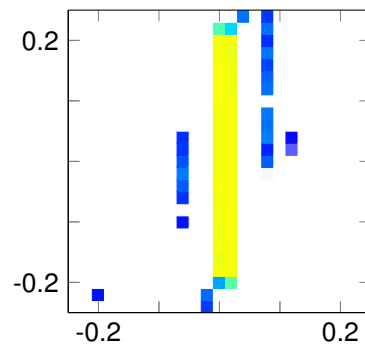
Figure 6.3: Conventional beamform incoherent line source



(a) 5000Hz



(b) 10000Hz



(c) 20000Hz

Figure 6.4: DAMAS incoherent line source

7. Array Calibration Function

Experience learns the conventional beamforming technique is not capable of accurately estimating the strength of line sources. Using simulated line sources it can be noticed the peak levels of the spectral maps are sometimes a value of 15dB too high.

To cope with this problem, an array calibration function (ACF) is designed. A synthetic CSM with a line source of known strength is used for the conventional beamforming algorithm. The difference between beamforming output and source strength is the same for line sources of various strength levels. This difference can be used to correct the peak levels of wind tunnel experiments.

The line source is simulated with 64 equidistant monopoles, over a length of 0.4m. The use of 64 monopoles makes it possible to form multiple coherent groups, and thus simulating different coherent lengths. The strength of the monopoles is set at 100dB. The ACF value is the source strength minus the beamforming peak level, therefore in wind tunnel experiments, adding the ACF value to the results, gives the correct peak value.

Since the ACF is in dB scale, the strength of the modeled sources isn't influencing the ACF value. Subtracting the average microphone pressure makes the ACF also independent of the number of sources used to model the line source. The only parameters influencing the ACF are wind tunnel dimensions and of course frequency and coherence length.

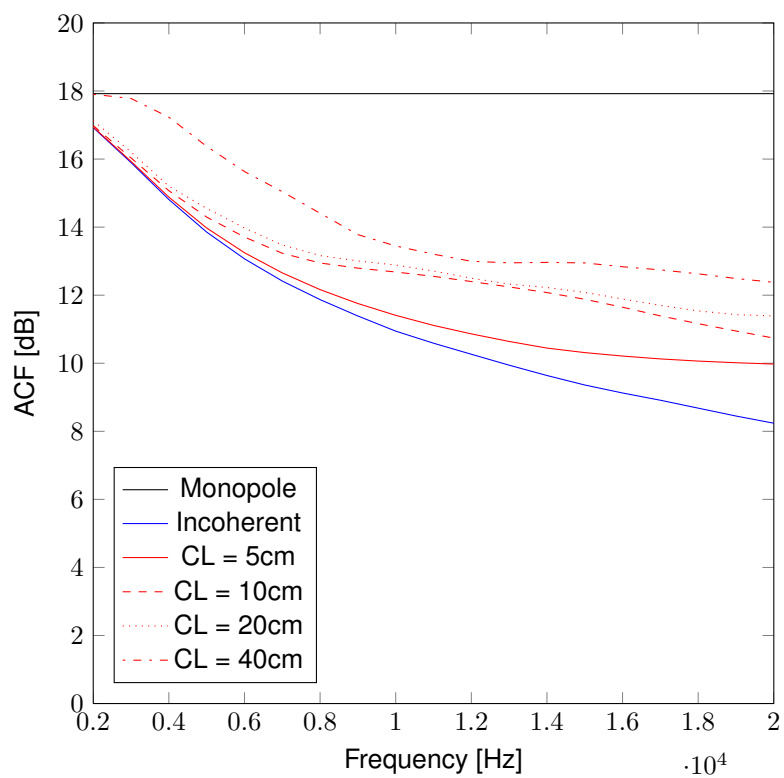


Figure 7.1: Array Calibration Function for various coherence lengths

8. Determination of coherence levels

To use the array calibration function (chapter 7) on a signal measured at wind tunnel experiments, it is required to know the coherence length of the sources in the experiment. To determine the sound coherence length, the coherence is calculated between different scanning points of the acoustic source plot. This coherence can be found by a modification of the conventional beamforming algorithm [3]. The conventional beamforming algorithm is given by:

$$\frac{\hat{e}^T \hat{G} \hat{e}}{(\hat{e}^T \hat{e})^2} \quad (8.1)$$

For the determination of coherence levels, the beamforming algorithm is modified to use two different scanning points.

$$\frac{|\hat{e}^T \hat{G} \hat{d}|^2}{(\hat{e}^T \hat{G} \hat{e})(\hat{d}^T \hat{G} \hat{d})} \quad (8.2)$$

In this equation \hat{d} is the steering vector for a second scan point. This way the coherence level between two different points can be calculated. If one of these points is kept as a reference point, and the other is varied over the grid, coherence plots can be made.

8.1 Incoherent monopoles

This method is first used on a simulation with two incoherent monopoles. The results of this simulation are given in figure 8.1. The first monopole source is marked with an X , and is also the reference point. The second monopole source is a mirror of the first source over the y -axis.

It can be seen that when scanning frequency increases and thus beamwidth decreases, the source distribution becomes more visible. For the low frequencies (1500Hz and 2000Hz), the scanning resolution is too low to distinguish the two different sources. For higher frequencies the different sources can be seen.

The high coherence levels around the two sources are due to the fact that sidelobes, although they have a low level in the conventional source plot, are fully coherent with the original source. This indicates that the coherence plots may be used to identify sidelobes in acoustic source plots [1].

8.2 Line source

This coherence simulation is repeated with a 40cm line source which have different coherent lengths. Figure 8.2 shows the result of the simulation with

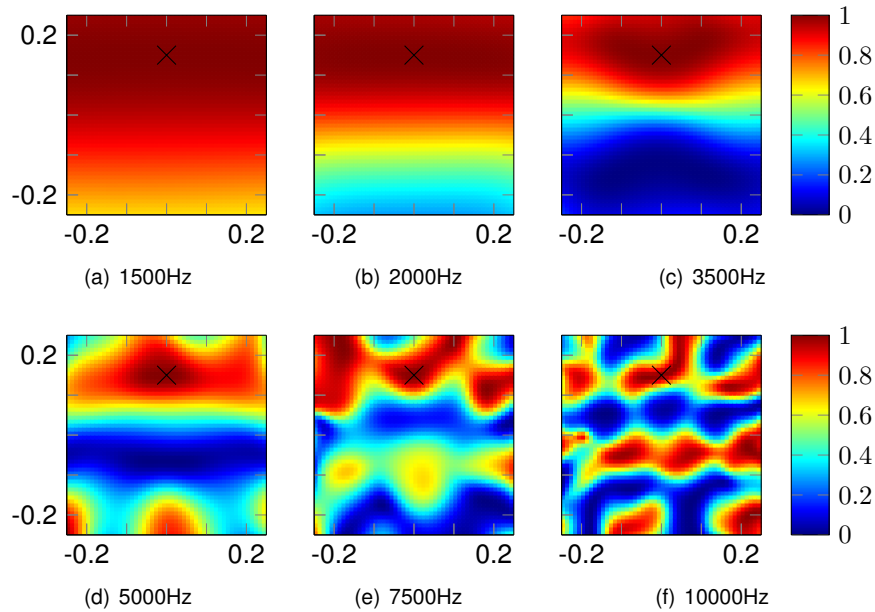


Figure 8.1: Coherence plots for different scanning frequencies

a frequency of 5000Hz. The results of the 10000Hz simulation are shown in figure 8.3. Figure 8.4 shows the 20000Hz simulation results.

At all three frequencies we can see quite big distinctions between the different coherent lengths. However, for the incoherent case and the 5cm coherence length the plots are quite similar. In the Array Calibration Function (Chapter 7) the difference in calibration values between the incoherent case and the 5cm case is around 2dB at higher frequencies. Therefore the ACF has an uncertainty of 2dB.

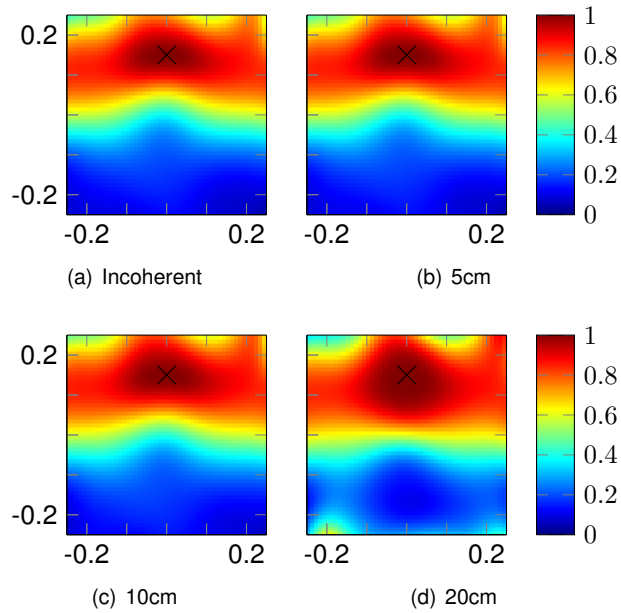


Figure 8.2: Coherence plots 5000Hz

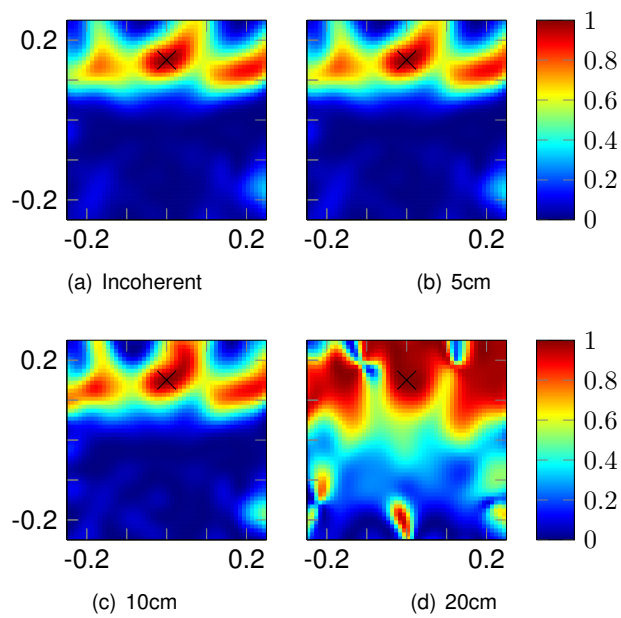


Figure 8.3: Coherence plots 10000Hz

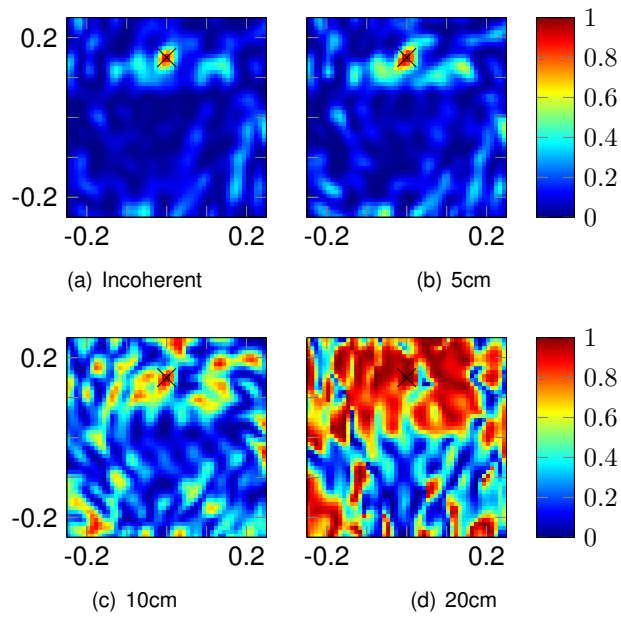


Figure 8.4: Coherence plots 20000Hz

9. Conclusion

During this internship period information is gained on the behaviour of acoustic source plots generated by beamforming and DAMAS algorithms. It is found that when investigating source strength by using peak levels, the levels are not giving the right results. The value of this off result differs for various coherence lengths.

Since DAMAS deconvolution method peak levels converge to the peak levels of conventional beamforming, the off result of both methods is the same.

An array calibration function is made, which calibrates the peak levels of conventional beamforming and DAMAS, to give no off result. The ACF is independent of source strength and number of sources used to simulate a line source. Coherence length and frequency are the two variables.

To extract coherence length from experimental results a modified beamforming algorithm is used. This method however, does not give absolute certainty about the coherence length. Since the coherence length of experimental results is not absolutely sure, the wrong calibration curve of the ACF can be picked, which can lead to an error up to 2dB.

The ACF and coherence length extraction method aren't tested on experimental results, since no experimental data was available at the time. For further research it is recommended to test both methods on experimental data for validation purposes.

9.1 Postscript

This internship period has been a valuable experience. Good insight in the activities involved in experimental research is obtained. A lot has been learned on beamforming characteristics and working with high end wind tunnel equipment.

I would like to thank Harry Hoeijmakers, Micael Carmo and Marcello Medeiros for making this internship possible. Furthermore I would like to thank Carlos Paganni for the daily supervision and enjoyable time at the wind tunnel experiments.

BIBLIOGRAPHY

- [1] S. Oerlemans & P. Sijtsma, Determination of absolute levels from phased array measurements using spatial source coherence. AIAA paper 2002-2464 2002.
- [2] Kjell J. Gåsvik, Optical Metrology, third edition. West Sussex: John Wiley & Sons Ltd. 2002.
- [3] Horne, C., Hayes, J.A., Jaeger, S.M., and Jovic, S., Effects of distributed source coherence on the response of phased arrays, AIAA paper 2000-1935, 2000.
- [4] Brooks, T.F. and Humphreys, W.M., A deconvolution approach for the mapping of acoustic sources (DAMAS) determined from phased microphone arrays, Journal of Sound and Vibration 294, 2006.
- [5] Oerlemans, S., Detection of aeroacoustic sources on aircraft and wind turbines thesis University of Twente, Enschede 2009.